SIAM J. APPL. MATH.
Vol. 62, No. 4, pp. 1197–1221

REGULAR TRAVELING WAVES IN A ONE-DIMENSIONAL NETWORK OF THETA NEURONS*

REMUS OSAN†, JONATHAN RUBIN‡, AND BARD ERMENTROUT‡

Abstract. This paper focuses on regular traveling waves, or waves that propagate smoothly, in a one-dimensional network of theta neurons. We show that when coupling strength is sufficiently large, there exist two traveling wave solutions for this network. Moreover, the cells in the network spike more than one time after joining the wave; that is, some form of synaptic depression or other adaptive mechanism must exist to attain single-spike traveling waves. We also present results about how the behavior of solutions to this network depends on the maximal synaptic coupling strength and the wave speed. This is relevant to consideration of uniqueness and to bounding the range of coupling strengths for which waves exist.

Key words. traveling waves, neuronal medium, synaptic coupling, theta model

AMS subject classifications. 34B08, 34C15, 34C37, 45J05, 92C20

PII. S0036139901387253

1. Introduction.

Traveling waves have received a great deal of recent theoretical treatment due to the ability of experimentalists to visualize them with multielectrode recordings and imaging methods. In a typical experiment, a slice of pharmacologically treated brain is electrically stimulated. Under a variety of circumstances, this results in the propagation of electrical activity in the form of a traveling wave [2, 9, 12, 13, 15, 21, 23]. When the wave reaches a neuron, the neuron generates an action potential, meaning that its transmembrane potential undergoes a brief, significant increase and decrease. Analogous wave-like spread of activity has been observed in intact animal brains, although it is considerably harder to obtain spatially distinct measurements in that setting [16].

The waves observed in brain slices are a consequence of synaptic interactions and the intrinsic behavior of the local neuronal circuitry. There are many computational models for these waves [3, 8, 9, 18, 19, 22], which differ from classic models of waves in excitable media in several key ways. Most importantly, in synaptically mediated propagation, the interactions are indirect and spatially extensive. More specifically, interaction occurs through the release of a synaptic transmitter, which occurs only when the neuron generates an action potential (or fires); furthermore, a given neuron can connect to many neurons over a substantial spatial distance. This contrasts with standard excitable media, in which interactions are mediated by diffusion (local) and depend directly on gradients in the potential or concentration of chemicals.

In general, computational models for synaptically coupled networks of neurons

*Received by the editors April 3, 2001; accepted for publication (in revised form) September 27, 2001; published electronically April 10, 2002.

http://www.siam.org/journals/siap/62-4/38725.html

†Department of Physics and Astronomy, University of Pittsburgh, Pittsburgh, PA 15260 (remus@phyast.pitt.edu). The research of this author was partially supported by NSF grant DMS-9972913.

‡Department of Mathematics, University of Pittsburgh, Pittsburgh, PA 15260 (rubin@math.pitt.edu, bard@math.pitt.edu). The research of the second author was partially supported by NSF grants DMS-9804447 and DMS-0108857. The research of the third author was partially supported by NSF grant DMS-9972913 and by the NIMH.

have the following form:

$$\begin{aligned} C\frac{dV_j}{dt} &= -I_{ion}(V_j(t), w_j(t)) - \left(\sum_k g_{jk} s_k(t)\right)(V_j - E_{syn}) + I_e, \\ \frac{dw_j}{dt} &= \frac{w_\infty(V_j) - w_j}{\tau_w(V_j)}, \\ \frac{ds_j}{dt} &= a(V_j)(1 - s_j) - s_j/\tau_s. \end{aligned}$$

Here $V_j(t)$ is the transmembrane potential of a cell at position j in the network. There may be dozens of variables like w_j for each cell, representing the different ion channels which make up the action potential. The synaptic gates s_j are the only way in which the neurons are able to communicate to each other. The function $a(v)$ is zero unless the neuron fires an action potential (which lasts only briefly). During the action potential, a is roughly constant and large. Thus $s_j(t)$ is often approximated for $t \geq 0$ by a simple difference of exponentials:

$$s_j(t) \approx e^{-t/\tau_s} - e^{-a_{max}t},$$

where a_{max} is the value of a at the peak of the action potential. If a_{max} is large, an even simpler approximation is $s_j(t) = e^{-t/\tau_s}$ for $t \geq 0$. There can be more than one population of neurons, however, and thus even with such approximations the full system of equations for a network can become quite complicated.

The most obvious simplification one can make is to assume that the system is spatially homogeneous, so that $g_{jk} = g_{|j-k|}$. In order to look for traveling waves, one generally takes the continuum limit, so that the synaptic interaction over a spatial domain Ω can be written simply as

$$I_{syn}(x,t) = \left(g_{syn} \int_\Omega J(x-y)s(y,t)\ dy\right)(V(x,t) - E_{syn}),$$

where g_{syn} denotes maximal synaptic conductance. Simulations of these models show that they appear to support traveling waves of a fixed speed and, furthermore, that the speed and properties of these waves are in the right physiological range to explain the experimental observations.

Several investigators have recently attempted to study the existence and stability of waves in related models using rigorous and formal asymptotic methods. Ermentrout [6] and Bressloff [1] considered a simplified model in which the dynamics of the individual uncoupled neuron has the simple form:

$$I_{ion} = g_l(V - E_l).$$

Whenever the neuron crosses a fixed potential $V = V_T$, it "fires a spike" and is reset to V_{reset}. This model is called the leaky integrate-and-fire (LIF) model. By assuming that during the wave only the first spike matters, both authors were able to write down closed form expressions for the velocity of propagating waves. As with the classic action-potential models (cf. [17]), two different waves exist for fixed parameter values: a fast wave which is stable and a slow wave which is unstable. More recently, Golomb and Ermentrout [10] have extended this work to cases in which there are delays in synaptic transmission as well as to models incorporating two types of neurons.

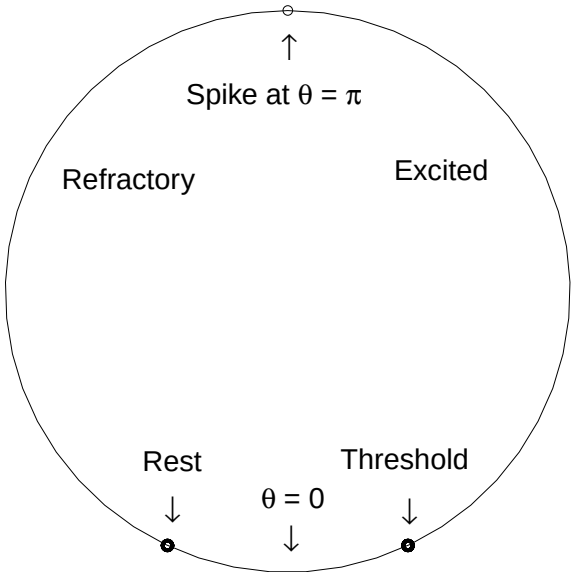

FIG. 1. *The theta neuron regimes for $\beta = -0.05$ and $I = 0$. The circular phase space for θ is displayed, with $\theta = 0$ at bottom and $\theta = \pi$ at top. "Rest" and "threshold" indicate the fixed points θ_{rest} and θ_T for θ, while θ is considered to be excited on (θ_T, π) and refractory on (π, θ_{rest}).*

A recent alternative to the LIF model, called the "theta" model, arises in certain limits from a whole class of biophysically based neural models [5, 7, 11]. In particular, if one of these model neurons is tuned to sit close to its threshold for firing an action potential, then its dynamics can be rigorously mapped to dynamics on the unit circle of the following form:

$$\frac{d\theta}{dt} = 1 - \cos\theta + (1 + \cos\theta)Z(t).$$

Here θ parameterizes the circle, and Z represents all inputs to the neuron. Under the transformation leading to the theta model, the synaptically coupled network is reduced to a scalar model:

$$\frac{\partial\theta(x,t)}{\partial t} = 1 - \cos\theta(x,t) + (1 + \cos\theta(x,t))\left[\beta + g_{syn}\int_\Omega J(x-y)s(y,t)\,dy\right], \tag{1}$$

where $\beta \in (-1, 0)$ is a bias parameter that controls the excitability of the cell and $s(x,t)$ satisfies an ordinary differential equation in time. Since it is obtained via a rigorous transformation, the theta model is continuous, unlike the LIF model. Correspondingly, the theta model retains information lost in the LIF model, particularly the delay between the crossing of the spiking threshold and the actual firing of an action potential; Figure 1 shows the approximate mapping of the theta model to the potential of an active neuron when $Z = \beta + I$, a fixed negative number. The treatment of this model in this paper is likely to give hints on how to approach the existence of traveling waves in biophysically based models.

The goal of the present paper is to prove the existence of traveling waves in the simplified system (1) on $(x,t) \in \mathbb{R} \times \mathbb{R}$. In general, these waves may involve single or multiple spikes fired by each cell; in the waves we find, we show that each cell fires

multiple spikes, but we do not further characterize the behavior of cells after they fire their initial spikes. In section 2, we describe the theta model in more detail and introduce additional simplifications. Section 3 contains the bulk of the mathematical results including the existence proof. In section 4, we numerically explore how waves depend on the maximal synaptic coupling strength g_{syn} and the wave speed c, and we also obtain some rigorous estimates about how coupling strength and wave speed interact to produce traveling waves. Generalizations and further discussion finish out the paper.

2. Regular traveling wave solutions in the theta model.

2.1. The single-cell model. Equation (1) for a theta neuron can be rewritten as

$$\frac{d\theta}{dt} = (1-\cos\theta) + (1+\cos\theta)(\beta + I(t)), \tag{2}$$

where θ is the phase variable and $I(t)$ denotes the time-dependent inputs to the neuron. When θ increases through $(2n+1)\pi$ for any integer n, we say that the theta neuron fires a spike. If we fix I such that $I+\beta<0$, then there is a stable rest state. If $I+\beta>0$, then the neuron fires with period $\pi/\sqrt{I+\beta}$. Assuming no external current, the stable rest state is given by

$$\theta_{rest} = -\cos^{-1}\left(\frac{1+\beta}{1-\beta}\right), \qquad \beta<0. \tag{3}$$

For the solitary neuron, if θ exceeds a threshold value θ_T, then based on (2) it will reach the value π corresponding to a spike. θ_T is an unstable rest state given by the following equation:

$$\theta_T = \cos^{-1}\left(\frac{1+\beta}{1-\beta}\right), \qquad \beta<0. \tag{4}$$

Figure 1 shows the different regimes for the θ-neuron. For this and all subsequent figures, $\beta=-0.05$.

2.2. Regular traveling waves and coupling. We can generate a traveling wave if we allow each cell in a one-dimensional network to send a signal to the neighboring cells. We assume that the coupling is synaptic and that the strength of the coupling is proportional to a decaying weight function $J(x)$ of the distance between two cells in the network. Biologically relevant forms for the weight function include Gaussian, exponential, and step functions. When synaptic coupling is introduced as an input into (2), (1) is obtained:

$$\frac{\partial\theta(x,t)}{\partial t} = (1-\cos\theta(x,t)) + (1+\cos\theta(x,t))(\beta + g_{syn}J*s), \tag{5}$$

where $J*s$ denotes the convolution $\int_\Omega J(x-y)s(y,t)\,dy$ and $(x,t)\in\mathbb{R}\times\mathbb{R}$. Figure 2(a) shows the time-evolution of a solitary spike solution for fixed x, generated by solving (5) together with the corresponding ordinary differential equation in time for s (see [14]). The time-evolution of s for this solution is plotted in Figure 2(b).

Figure 3 shows a simulation from [14] of two different types of traveling waves in a discretized network of 150 cells. In each, the first cell (upper left corner) is given an initial depolarization (that is, the θ value is set above threshold for this cell),

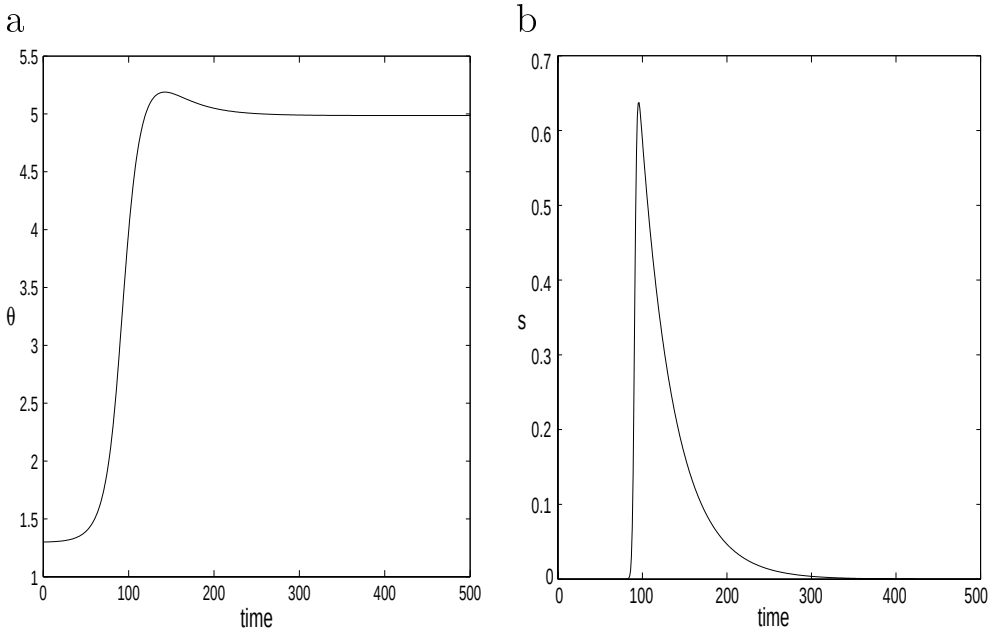

FIG. 2. *Evolution of* (a) θ *and* (b) *synaptic variable* s *versus time for a solitary spike solution. Note that a spike occurs when* θ *crosses through* π*, around time* 90.

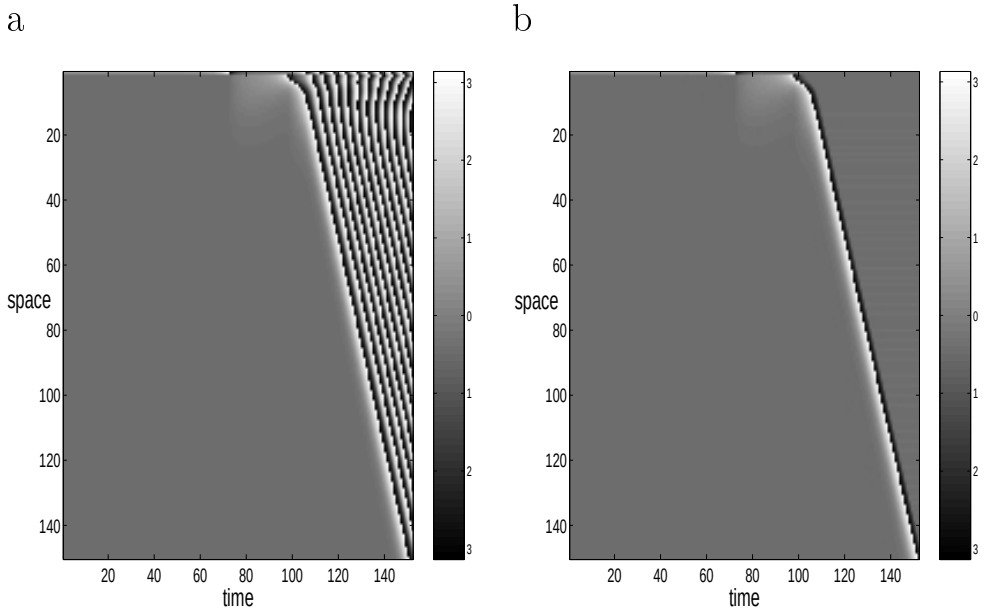

FIG. 3. *One-dimensional regular traveling waves. In* (a)*, the first cell spikes around time* 100 *msec; this induces a wave of spiking throughout the network (the leftmost light band in the figure). Subsequently, all excited cells spike repeatedly. In* (b) *each cell fires only a single spike once excited.*

initiating a wave. Time is represented on the horizontal axis, while the line of 150 cells is represented on the vertical axis. No input comes in to the cells across the boundaries. The phase of the cells is coded in gray scale, and spiking occurs when the color of the cells becomes white (for illustration purposes the phase is represented from $-\pi$ to π). In the first wave, cells spike repeatedly after joining the wave. The second is a single-spike wave in which each cell spikes once and then returns to rest; this is achieved numerically by blocking all spikes after the first. Note that the initial conditions induce transient changes in wave speed before constant speed propagation develops. Also, the cells near the top of the plot do not receive full input because they lie near the upper boundary of the simulated region; this slows their spiking and causes the curvature seen in the upper right part of Figure 3(a).

In [14], it is shown that additional spikes fired by each cell, after the first spike, contribute only negligibly to the wave speed. However, these spikes may affect the temporal evolution of s. Our strategy for consideration of traveling waves will be the following. Assume that a single-spike traveling wave exists. We can compute the time-evolution of s at each x, as shown in Figure 2(b), and then use this to compute the time-dependent synaptic input $J * s$ to each cell in the network. Note that in a multiple-spike traveling wave, the amount of synaptic input to each cell is greater than that for the single-spike wave. Thus, to prove the existence of some form of traveling wave, it suffices to check the consistency condition that each cell really does fire when it receives the single-spike synaptic input. In subsections 3.1–3.3 we show that this condition holds. Given this, if each cell returns to rest after firing one spike upon receiving this input, then a single-spike wave truly exists. Otherwise, some form of multiple-spike wave exists; that is, each cell receives sufficient input to generate a spike, but we do not know exactly how much input it receives or how many times it spikes. We show in subsection 3.4 that the multiple-spike scenario actually occurs; see also Remark 3.1.

We will employ the same traveling wave formulation used in [6]. Traveling wave solutions satisfy $\theta(x,t) = \theta(\xi)$ and $s(x,t) = s(\xi)$ for $\xi = ct - x$ for some constant speed c. As discussed in the introduction, we approximate s, which satisfies an ordinary differential equation, by a function $\alpha(t - x/c) = \alpha(\xi/c)$. We assume that each cell spikes at $\xi = 0$. The net input to a cell at position ξ will be $J * s = \int_0^\infty d\xi' J(\xi - \xi')\alpha(\xi'/c)$, and thus the θ-equation (5) becomes

$$c\frac{d\theta}{d\xi} = (1-\cos\theta)+(1+\cos\theta)\left[\beta + g_{syn}\int_0^\infty d\xi' J(\xi-\xi')\alpha(\xi'/c)\right], \quad \xi \in (-\infty,\infty). \tag{6}$$

We make the following assumptions on $J(x), \alpha(t)$, in addition to integrability:

$$\text{(H1)} \begin{cases} J(x) = J(-x), \\ J(x) \geq 0, \\ \frac{dJ}{dx} < 0 \text{ for } x > 0, \end{cases}$$

$$\text{(H2)} \begin{cases} \alpha(t) = 0 \text{ for } t < 0, \\ \alpha(0) \geq 0, \\ \alpha(t) > 0 \text{ for } t > 0, \\ \alpha(t) \text{ has a single maximum.} \end{cases}$$

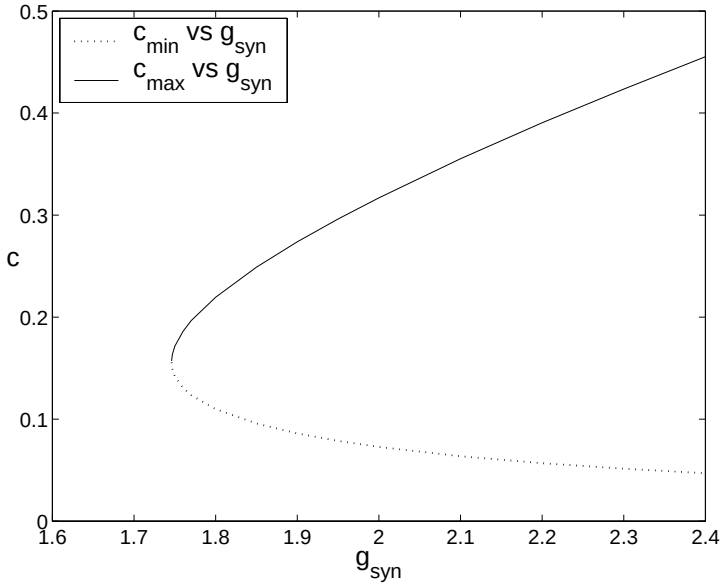

FIG. 4. *Numerical solution of* (6) *using a shooting procedure yields two branches of traveling wave solutions satisfying* (i), (ii) *for* g_{syn} *sufficiently large, namely,* $g_{syn} > 1.746$. *Numerics indicate that only the top branch (larger* c*) is stable.*

Single-spike traveling wave solutions of (5) are solutions of (6) that satisfy the following conditions:

(i) $\theta \to \theta_{rest}$ as $\xi \to -\infty$;

(ii) $\theta(0) = \pi$;

(iii) $\theta \to \theta_{rest} + 2\pi$ as $\xi \to \infty$.

General traveling wave solutions need only satisfy (i) and (ii). Note that there is no closed form analytic solution to the boundary value problem posed by (6) plus (i)–(ii). We will show that under (H1) and (H2), for g_{syn} sufficiently large, there are at least two values of c such that for each there exists a solution to (6) satisfying (i) and (ii); to do this, we consider (6) on $\xi \in (-\infty, 0]$. This existence is illustrated numerically in Figure 4. We next show that (iii) cannot hold for these solutions. Thus, while traveling wave solutions exist, each cell spikes more than once in these waves, and the wave speeds differ from the two values found initially. Correspondingly, some form of synaptic depression or other adaptive mechanism must be introduced to generate single-spike traveling waves. For the waves found here, we cannot determine how many spikes each neuron fires, since the form of α that we have assumed (e.g., with a single maximum) becomes invalid when multiple spikes occur. We also do not prove that only two waves exist. In section 4, however, we give results which suggest that for appropriate J and α there are exactly two solutions to (6) satisfying (i) and (ii).

We rewrite (6) as

$$c\frac{d\theta}{d\xi} = f(\theta) + g_{syn}\ g(\theta)h(\xi, c), \tag{7}$$

where $f(\theta) = (1 - \cos\theta) + (1 + \cos\theta)\beta$, $g(\theta) = (1 + \cos\theta)$, and $h(\xi, c) = \int_0^\infty d\xi' J(\xi - \xi')\alpha(\xi'/c)$. The graphs for $f(\theta)$ and $g(\theta)$ are shown in Figure 5. Note that $f(\theta) < 0$

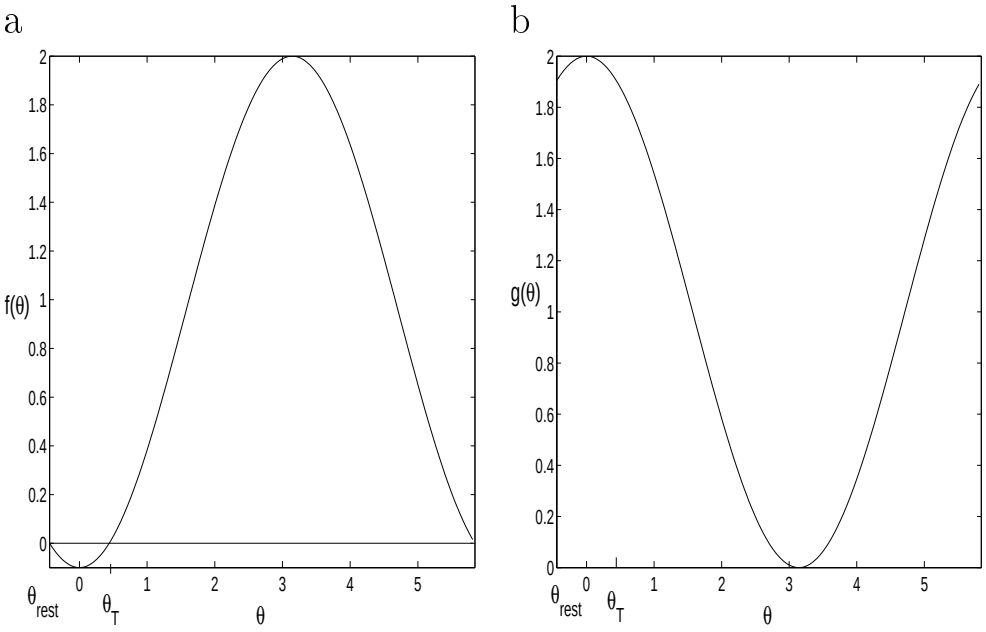

FIG. 5. (a) $f(\theta)$, (b) $g(\theta)$.

for $\theta \in (\theta_{rest}, \theta_T)$, and $f(\theta) \geq 0$ for the rest of the domain (mod 2π); we will also use that $f(\theta) > 2\beta$.

The main result of this paper is the following.

THEOREM 2.1. *If* $(H1)$, $(H2)$ *hold, then for* g_{syn} *sufficiently large there exist two traveling wave solutions to* (5). *These are multiple-spike waves; that is, an adaptation mechanism such as synaptic depression must be included for single-spike wave solutions to* (5) *to exist.*

In section 3, we prove this result for the special case that $\alpha(t) = A_0 e^{-a_t t}$ for $t > 0$ and $J(x) = e^{-a_x|x|}$, for concreteness in the relevant calculations. In section 5, we show that our proof generalizes beyond this specific $\alpha(t)$ and $J(x)$.

3. Proof of existence of traveling waves with multiple spikes. Since we seek traveling waves, we consider (7). Henceforth, we substitute the special forms of α and J mentioned in section 2, namely, $\alpha(t) = A_0 e^{-a_t t}$ for $t > 0$ and $J(x) = e^{-a_x|x|}$. Since the existence of waves is not affected by rescaling $\xi = ct - x$ through multiplication by a nonzero constant, we see that the wave speed c is proportional to $1/a_x$, and we can without loss of generality rescale x and take $a_x = 1$, with a corresponding rescaling of c. For clarity, we also set $a_t = 1$. This is not the general case, since (7) is derived from ordinary differential equations in t; however, the parameter a_t can be inserted in the arguments below without any complications. Figure 6 shows how wave speed changes with the decay rates a_t and a_x of α and J in numerical simulations, with c given as a function of a_t for $a_x = 1$ in Figure 6(b).

We compactify from the infinite domain $(-\infty, 0]$ to the compact one $[0, 1]$ using the transformation $\eta = e^{\xi}$. The θ-equation (7) thus becomes

$$c\,\eta\,\frac{d\theta}{d\eta} = f(\theta) + A_0 g_{syn}\; g(\theta)\frac{c}{1+c}\;\eta. \tag{8}$$

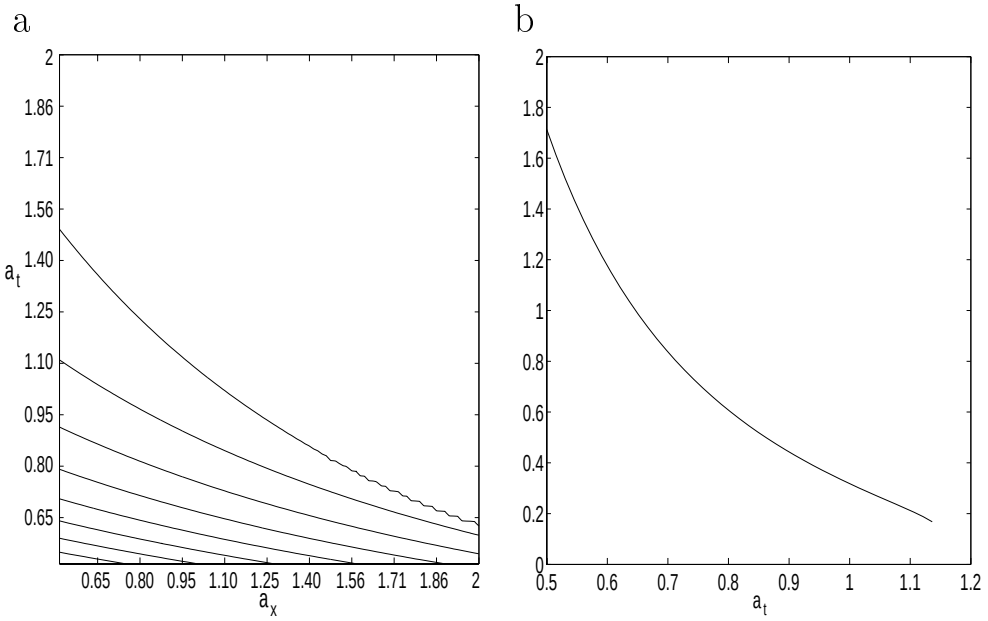

FIG. 6. *Wave speed c for a range of decay rates of $\alpha(t) = e^{-a_t t}$ and $J(x) = e^{-a_x|x|}$. Speeds are computed numerically, with $g_{syn} = 2$, as the values for which conditions* (i) *and* (ii) *of section* 2 *hold, giving spiking.* (a) *The speed contours shown decrease from the lower left corner of the plot, in uniform steps from* 1.9628 *on the lowest contour to* 0.2454 *on the uppermost contour. To the right of the uppermost contour, waves cease to exist. The values displayed correspond to the faster of the two speeds found for which* (i) *and* (ii) *hold for each fixed a_t, a_x.* (b) *Plot of speed versus a_t for $a_x = 1$. Note that for a_t sufficiently large, the wave ceases to exist, so the curve terminates at a nonzero minimum speed (see also Figure* 4*).*

This formulation is useful for direct estimation of θ values along solutions, done in subsections 3.1 and 3.3. We can also write (8) as an autonomous system:

$$\begin{aligned} c\frac{d\theta}{d\xi} &= f(\theta) + A_0 g_{syn}\ g(\theta)\frac{c}{1+c}\eta, \\ \frac{d\eta}{d\xi} &= \eta. \end{aligned} \tag{9}$$

Note that the compactification procedure allows the rest points of (8) to be preserved in the autonomous formulation (9). Since the terms A_0, g_{syn} appear in (8), (9) only as a product, we henceforth without loss of generality set $A_0 = 1$ unless otherwise noted.

Under the flow of (9), we will follow the branch of the unstable manifold of $(\theta, \eta) = (\theta_{rest}, 0)$ that points into $\{(\theta, \eta) : \theta \geq \theta_{rest}, \eta > 0\}$. We will call this solution $(\theta^u(\xi), \eta^u(\xi))$. Calculation of the unstable eigenvector shows that (θ^u, η^u) lies outside of the θ nullcline given by $d\theta/d\xi = 0$, and thus we have $d\theta/d\xi > 0$ along this solution. In this formulation, traveling wave solutions result when (θ^u, η^u) passes through $(\pi, 1)$, corresponding to $\theta^u(0) = \pi$.

Here is the sketch of the proof of existence of traveling waves: we first show that for fixed $c = c_0 > 0$, for sufficiently large values of g_{syn}, we have $\theta^u(0) > \pi$. We will refer to this as overshoot. We next show that for fixed g_{syn} sufficiently large to give overshoot with $c = c_0$, in the limits $c \to 0$ and $c \to \infty$, we have $\theta^u(0) < \pi$. We

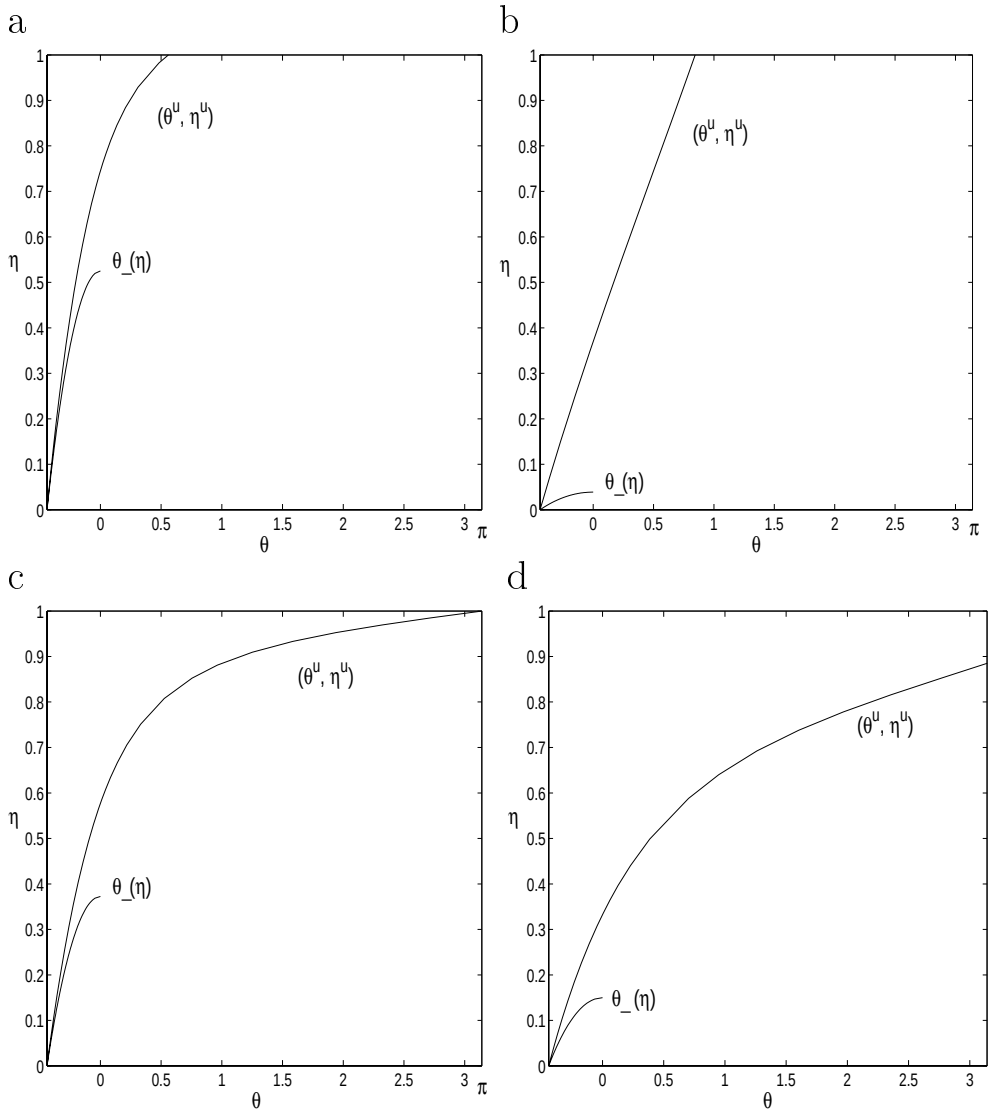

FIG. 7. *Shooting in* (θ, η)*-space:* (a) *undershooting for a small velocity* $c_s = 0.05$, (b) *undershooting for a large velocity* $c_l = 1$, (c) *one of the solutions at* $c_* = 0.072$, *and* (d) *overshooting for some intermediate velocity* $c_i = 0.2$ *(*$c_s < c_* < c_i < c_l$*). Note that, for small velocities,* θ *remains close to one branch of the* θ*-nullcline (labeled* $\theta_-(\eta)$ *here) until* θ_- *is annihilated at* $\theta = 0$*, but the close tracking is lost when the speed increases. In all four plots,* $g_{syn} = 2$.

will refer to this as undershoot. Therefore, based on continuity, for our fixed g_{syn} there exist at least two values of c for which $\theta^u(0) = \pi$. One corresponds to a slow solution, which is numerically unstable, and the other one to a fast solution, which is numerically stable. This is summarized in the simulation results shown in Figure 7.

3.1. Overshoot. We will show that for an arbitrary fixed value of c, which we call c_0, we can choose the synaptic constant g_{syn} so that $\theta^u(0) > \pi$. If one integrates (8), a singularity may arise at $(\theta_{rest}, 0)$. To avoid this, we compare (θ^u, η^u) to a

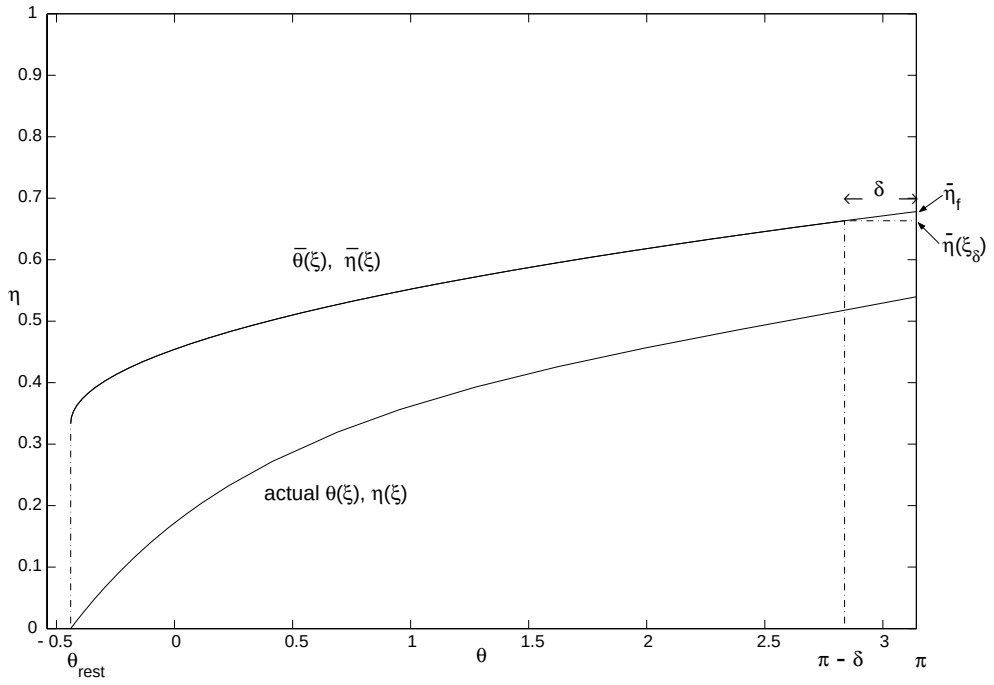

FIG. 8. *The solution* $(\bar{\theta}, \bar{\eta})$*, which passes through* $(\theta_{rest}, 1/3)$*, used for proving that one can overshoot. The actual solution is bounded above by* $(\bar{\theta}, \bar{\eta})$ *as shown. Curves are plotted for* $g_{syn} = 3.5$*,* $c = 0.27$*.*

solution $(\bar{\theta}(\xi), \bar{\eta}(\xi))$ passing through $(\theta_{rest}, 1/3)$. To do so, we derive separate bounds on separate subintervals of the ξ domain, based on the forms of $f(\theta), g(\theta)$. (Note that $1/3$ was selected arbitrarily for definiteness; any number in $(0, 1)$ could have been used here, with corresponding adjustments below.)

More precisely, we use $(\bar{\theta}(\xi), \bar{\eta}(\xi))$ to provide an upper bound on the value of η at which θ^u reaches $\pi - \delta$ for small $\delta > 0$ in the case of large g_{syn}, and we show that this bound is a monotone decreasing function of g_{syn}. Then we show that if we make this bound sufficiently small by increasing g_{syn}, then θ^u reaches π before η^u reaches 1. The intervals used for this are presented in Figure 8.

Clearly the value of η^u when $\theta^u = \pi$ is less than the η-value, call it $\bar{\eta}_f$, reached by the trajectory $(\bar{\theta}(\xi), \bar{\eta}(\xi))$ by the time $\bar{\theta} = \pi$ (see Figure 8). Thus, it suffices to show that $\bar{\eta}_f < 1$ for g_{syn} sufficiently large.

Fix a small $\delta > 0$. Define ξ_δ such that $\bar{\theta}(\xi_\delta) = \pi - \delta$; note that $\bar{\eta}(\xi_\delta) > 1/3$. Then, from (8), since $f(\theta) > 2\beta$ and $g(\theta) > 1 - \cos(\delta)$ over the interval of integration, it follows that

$$\begin{aligned} \pi - \delta - \theta_{rest} &> \int_{1/3}^{\bar{\eta}(\xi_\delta)} d\eta \left(\frac{2\beta}{\eta c_0} + g_{syn} \frac{1}{1 + c_0} (1 - \cos\delta) \right) \\ &= \frac{2\beta}{c_0} \ln(3\bar{\eta}(\xi_\delta)) + g_{syn} \frac{1}{1 + c_0} (1 - \cos\delta) \left(\bar{\eta}(\xi_\delta) - \frac{1}{3} \right). \end{aligned} \tag{10}$$

Rearranging (10), and then using $\beta < 0$ and $\bar{\eta}(\xi_\delta) > 1/3$, yields

$$\pi - \delta - \theta_{rest} + \frac{1}{3} g_{syn} \frac{1}{1 + c_0} (1 - \cos\delta)$$

$$
\begin{aligned}
(11) \qquad &> \frac{2\beta}{c_0}\ln(3\bar{\eta}(\xi_\delta)) + g_{syn}\frac{1}{1+c_0}(1-\cos\delta)\bar{\eta}(\xi_\delta) \\
&> \left[\frac{6\beta}{c_0} + g_{syn}\frac{1}{1+c_0}(1-\cos\delta)\right]\bar{\eta}(\xi_\delta).
\end{aligned}
$$

Fix g_{syn} sufficiently large that the right-hand side of (11) is positive. Then (11) gives us an upper bound on $\bar{\eta}(\xi_\delta)$. Moreover, it is easy to see that this upper bound decreases monotonically towards $1/3$ as g_{syn} increases.

For $\bar{\theta} \in (\pi-\delta, \pi]$, we have $0 < (1+\cos\delta) + (1-\cos\delta)\beta < f(\bar{\theta}) < 2$ and $g(\bar{\theta}) \geq 0$. Setting $f_0(\delta) = (1+\cos\delta) + (1-\cos\delta)\beta$, equation (8) gives

$$
(12) \qquad \pi - (\pi - \delta) > \int_{\bar{\eta}(\xi_\delta)}^{\bar{\eta}_f} d\eta \, \left(\frac{f_0(\delta)}{\eta c_0}\right).
$$

Integration transforms inequality (12) to the inequality

$$
\delta > \frac{f_0(\delta)}{c_0}\ln\left(\frac{\bar{\eta}_f}{\bar{\eta}(\xi_\delta)}\right).
$$

Thus, $\bar{\eta}_f < 1$ holds if $\bar{\eta}(\xi_\delta)\exp(\delta c_0/f_0(\delta)) < 1$. Since $f_0(\delta) \to 2$ as $\delta \to 0$, we can fix δ such that $\exp(\delta c_0/f_0(\delta)) < 2$. Then we can choose g_{syn} sufficiently large such that $\bar{\eta}(\xi_\delta) < 1/2$, yielding $\bar{\eta}_f < 1$. This gives the desired overshoot result.

Fix g_{syn} to be this large for the rest of section 3. We next show that for such g_{syn}, the unstable manifold (θ^u, η^u) of $(\theta_{rest}, 0)$ undershoots for $c \to 0$ and $c \to \infty$. That is, θ^u does not reach π before η^u reaches 1 in these limits.

3.2. Undershoot—small velocities. When $\eta = 0$, θ_{rest} and θ_T are given by (3) and (4), respectively. When η increases from 0 to some nonzero value, the branches of the θ-nullcline for system (9), which we denote $\theta_-(\eta)$ and $\theta_+(\eta)$, become closer to each other:

$$
\theta_-(\eta) = -\cos^{-1}\left(\frac{1+\beta+g_{syn}\frac{c}{1+c}\eta}{1-\beta-g_{syn}\frac{c}{1+c}\eta}\right) \leq 0, \quad \theta_+(\eta) = \cos^{-1}\left(\frac{1+\beta+g_{syn}\frac{c}{1+c}\eta}{1-\beta-g_{syn}\frac{c}{1+c}\eta}\right) \geq 0
\tag{13}
$$

for $\beta + g_{syn}\frac{c}{1+c}\eta < 0$; see Figure 9. Let

$$
(14) \qquad \eta_a(c) = \frac{-\beta(1+c)}{g_{syn}c}
$$

denote the η-value at which $\theta_-(\eta) = \theta_+(\eta) = 0$. The point $(0, \eta_a(c))$ is the knee of the θ-nullcline.

We can see from (13) that this nullcline, which bounds the negatively invariant region where $\frac{d\theta}{d\xi} < 0$, rises in (θ, η) phase space as $c \to 0$. For a suitable value of c, which we denote by c_1, $\eta_a = 1$, with $\eta_a > 1$ for $c < c_1$, as seen in Figure 9. Since the unstable manifold of $(\theta_{rest}, 0)$ is bounded to the left of this nullcline, where $\theta < 0$, for $\eta \leq \eta_a$, it certainly reaches $\eta = 1$ before reaching $\theta = \pi$ for $c \leq c_1$. Consequently, for speed less than or equal to c_1, no spiking can occur. Effectively, such a small propagation speed would not deliver enough synaptic input at any one time to cause neurons ahead of a wave to spike.

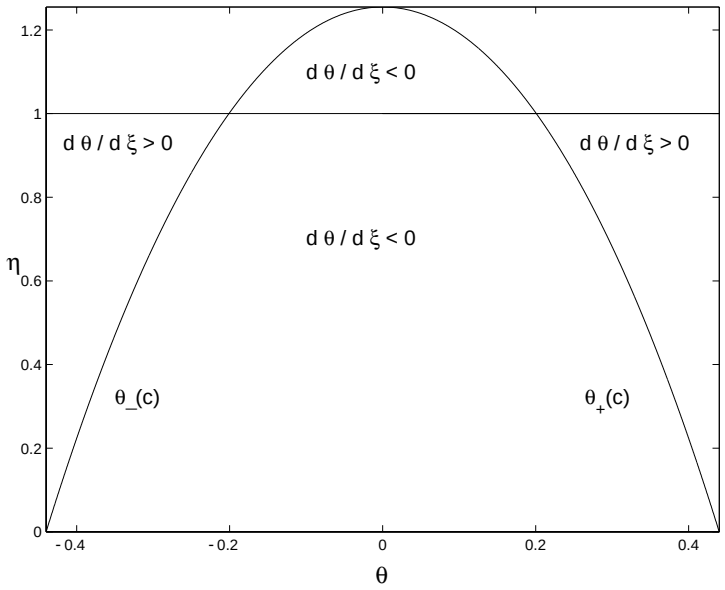

FIG. 9. *Undershooting for small velocities follows from the position of the θ-nullcline. This figure shows the nullcline for* $g_{syn} = 10$, $c = 0.004$.

3.3. Undershoot—large velocities. To prove that an undershoot occurs for large wave velocities, consider $c > c_0$, the speed at which overshoot was proved to occur in subsection 3.1. We know that for such c the knee of the θ-nullcline lies at $(0, \eta_a(c))$ with $\eta_a(c) < 1$. We will now show that for $c > c_0$ sufficiently large the trajectory of (8) starting from $(0, \eta_a(c))$ fails to reach $\theta_T < \pi$ by the time it achieves $\eta = 1$. Since $(\theta^u(\xi), \eta^u(\xi))$ is bounded to the left of this trajectory in the (θ, η) plane, this implies that $\theta^u < \pi$ when $\eta^u = 1$ for such c, giving the desired result.

Let η_T denote the η value at which the trajectory of (8) from $(0, \eta_a(c))$ reaches $\theta = \theta_T$; this is uniquely defined since $d\theta/d\eta > 0$ for $\theta > 0$ and $\eta > \eta_a(c)$. From (8) with initial condition $(0, \eta_a(c))$, we have

$$\theta_T < \int_{\eta_a(c)}^{\eta_T} d\eta \ \left(\frac{\max_\theta f(\theta)}{\eta c} + g_{syn} \frac{1}{1+c} \max_\theta g(\theta) \right), \tag{15}$$

where the maxima are computed over $[0, \theta_T]$. Since $f(\theta) \leq 0$ on this interval, and $g(\theta) \leq 2$, (15) yields

$$\theta_T < \int_{\eta_a(c)}^{\eta_T} d\eta \ g_{syn} \frac{2}{1+c} = \frac{2}{1+c} g_{syn} (\eta_T - \eta_a(c)). \tag{16}$$

Since $\eta_a(c) > 0$ for all speeds c, it is obvious from here that for sufficiently large c we have $\eta_T > 1$, giving the desired undershoot. That is, at high propagation velocities, a neuron ahead of a wave would not have time to integrate enough synaptic input to enable it to spike when the wave reached it, so wave propagation would not be possible.

3.4. Failure to return to rest after a single spike. Suppose we have $\theta^u(0) = \pi$, with $\theta^u(\xi) \to \theta_{rest}$ as $\xi \to -\infty$, by definition. Here we will show that in the spiking

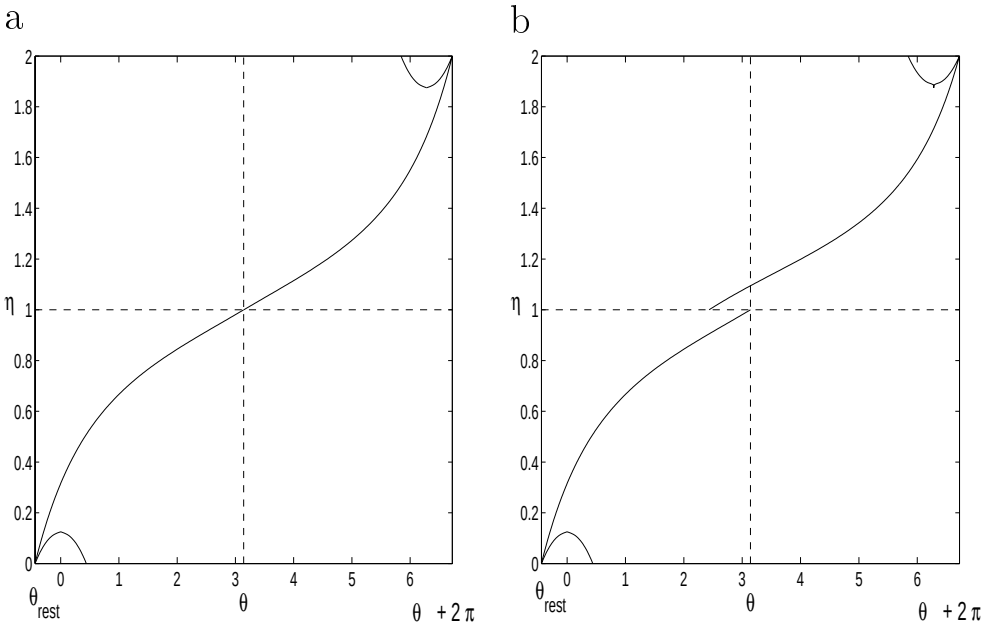

FIG. 10. *Numerical trajectories demonstrating the symmetry argument. For numerical and illustrative purposes, we have compactified phase space by defining* $\eta = e^{\xi}$ *for* $\xi \leq 0$*, and* $\eta = 2 - e^{-\xi}$ *for* $\xi > 0$*. In* (a)*, we show a traveling wave solution constructed with even coupling function* h_e*. In* (b)*, we show the stable manifold of* $\theta_T + 2\pi$ *and the unstable manifold of* θ_{rest}*. Curves are plotted with* $A_0 = 1, g_{syn} = 1.9$*, and* $c = 0.274$*.*

solution corresponding to this trajectory, cells fire more than one spike. To do this, we show that this trajectory is bounded away from $\theta_{rest} + 2\pi$ as $\xi \to \infty$. In this subsection, we allow A_0 to be an arbitrary parameter, since we consider h separately from g_{syn}.

Let $h_e(\xi, c)$ denote the even function defined by $h_e(\xi, c) = h(\xi, c)$ for $\xi \leq 0$, and $h_e(\xi, c) = h(-\xi, c)$ for $\xi > 0$. With coupling h replaced by h_e, by symmetry, $\theta^u(\xi) \to \theta_T + 2\pi$ as $\xi \to \infty$ as a solution of (7), as illustrated in Figure 10(a).

However, h is not even; instead, we can show the following.

PROPOSITION 3.1. $h(\xi, c) > h(-\xi, c)$ *for* $\xi > 0$.

Proof. We can compute exactly that

$$h(\xi, c) = \begin{cases} A_0 \frac{c}{1+c} e^{\xi}, & \xi < 0, \\ A_0 \left(-\frac{c}{c-1} e^{-\xi} + \frac{2c^2}{c^2-1} e^{-\frac{\xi}{c}} \right), & \xi > 0, c \neq 1, \\ A_0 (\xi + \frac{1}{2}) e^{-\xi}, & \xi > 0, c = 1. \end{cases} \tag{17}$$

Let $\xi > 0$; if $c \neq 1$, then we have

$$\begin{aligned} h(\xi, c) - h(-\xi, c) &= A_0 \left(-\frac{c}{c-1} e^{-\xi} + \frac{2c^2}{c^2-1} e^{-\frac{\xi}{c}} \right) - A_0 \frac{c}{1+c} e^{-\xi} \\ &= A_0 \left(e^{-\frac{\xi}{c}} - e^{-\xi} \right) \left(\frac{2c^2}{c^2-1} \right). \end{aligned} \tag{18}$$

For $c > 1$, $(e^{-\frac{\xi}{c}} - e^{-\xi}) > 0$ and $(\frac{2c^2}{c^2-1}) > 0$. For $c < 1$, $(e^{-\frac{\xi}{c}} - e^{-\xi}) < 0$ and $(\frac{2c^2}{c^2-1}) < 0$. Therefore, $h(\xi, c) - h(-\xi, c) > 0$.

For $\xi > 0$ and $c = 1$ we have

$$\begin{aligned} h(\xi,1) - h(-\xi,1) &= A_0 \left(\xi + \frac{1}{2}\right) e^{-\xi} - A_0 \ \frac{1}{2} \ e^{-\xi} \\ &= \ A_0 \ \xi \ e^{-\xi} > 0. \end{aligned} \tag{19}$$

This concludes the proof of the proposition.

As a result of Proposition 3.1, if we follow the one-dimensional stable manifold $\hat{\theta}^s$ of $\theta_T + 2\pi$ under the flow of (7) backwards in time, the coupling term $h(\xi, c)$, which is stronger than the symmetric even coupling h_e, yields $\hat{\theta}^s(0) < \pi$, as illustrated in Figure 10(b). Thus $\theta^u(\xi)$ does not converge to $\theta_T + 2\pi$, nor to $\theta_{rest} + 2\pi$; instead, either $\theta^u(\xi)$ converges to $2n\pi + \theta_{rest}$ for some integer $n \geq 2$ as $\xi \to \infty$ or $\theta^u(\xi) \to \infty$. Since in both cases θ^u crosses through 3π, and possibly other odd multiples of π, along the way, it follows that each cell in the network will spike more than once during the time evolution of the traveling wave solution.

Remark 3.1. The existence arguments of subsections 3.1–3.3 would hold if we replaced the single-spike form of h considered above with the form of input corresponding to a 2-spike traveling wave, a 3-spike traveling wave, or an n-spike traveling wave for any natural number n. As a result, two possibilities exist. One is that for each such n a similar calculation to that of the proof of Proposition 3.1 would give failure of the corresponding trajectory to converge to $\theta_{rest} + 2n\pi$, implying that in the actual waves that exist, cells fire infinitely many spikes. Otherwise, there exist heteroclinic connections from θ_{rest} to $\theta_{rest} + 2n\pi$ for some n, giving the existence of n-spike waves. The difficulty in completing the calculations needed to check which case holds lies in computing the times between consecutive spikes, as needed to specify h for $n > 1$.

4. Parameter-dependence of solutions.

4.1. Dependence of solutions on the velocity *c*. Numerical calculations suggest that the two solutions found in the previous section are the only two traveling wave solutions to (9), as illustrated in Figure 11.

In this subsection, we consider how the behavior of the unstable manifold (θ^u, η^u) depends on velocity c for fixed g_{syn} (with $A_0 = 1$, as previously). While we will not prove that there are at most two traveling wave solutions to (9), the analytical results in this subsection suggest why this is likely to be the case for natural forms of coupling. Essentially, the two competing trends that lead in section 3 to undershoot for small and large velocities, respectively, appear to limit the number of possible waves to two. We will also briefly discuss how certain forms of coupling function $h(\xi, c)$ in (7) might support the existence of additional traveling wave solutions to the corresponding autonomous systems (see Remark 4.1 below).

Consider the dynamics of the θ component of solutions to (9) on the $[0, 2\pi)$ circle. For each fixed ξ and $\eta = e^{\xi}$ up to some level, there are two fixed points of the θ-equation on the circle; together, these form the θ-nullcline for (9). Following our earlier notation, for every c there exists a point $(0, \eta_a(c))$ at which the nullcline for the θ-equation has a knee, or annihilates (see Figure 9). If we take η as a parameter in this θ-equation, then the equation's fixed points coalesce in a saddle-node bifurcation at $\theta = 0$ at $\eta = \eta_a(c)$, as given in (14).

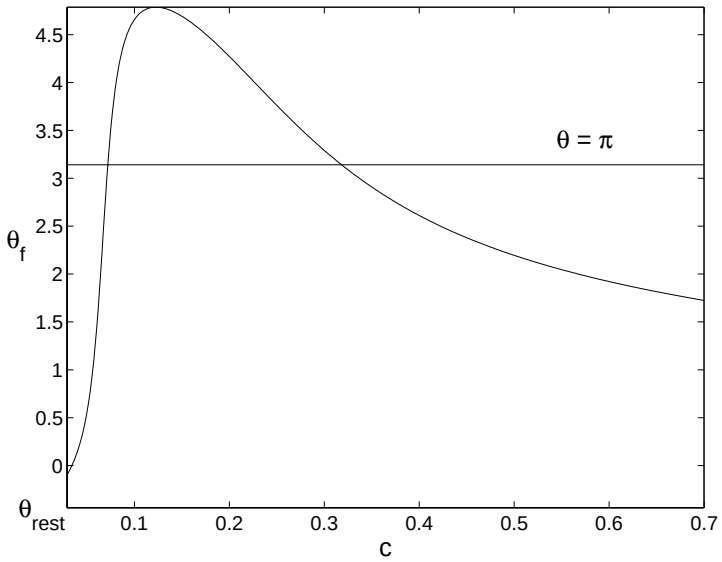

FIG. 11. *Numerically generated θ_f^u as a function of c for $g_{syn} = 1.9$. Here θ_f^u is defined as the value of θ^u when $\eta^u = 1$. The horizontal lines show $\theta = \pi$ and $\theta = \theta_{rest}$. Traveling wave solutions exist precisely when $\theta_f^u = \pi$.*

The unstable manifold (θ^u, η^u) is bounded to the left of the θ-nullcline, with $\theta < 0$, in (θ, η)-space until $\eta > \eta_a(c)$. Thus, a traveling wave can only possibly exist for c such that $\eta_a(c) < 1$, as used in subsection 3.2. For every such c value, define $\theta_a(c)$ as the θ-value such that $\theta^u = \theta_a(c)$ when $\eta^u = \eta_a(c)$. In what follows, we use $(\theta_a(c), \eta_a(c))$ as a reference point and consider how the evolution of phase θ depends on velocity c from that point onwards. The following preliminary result states that, for larger c, solutions are farther from the firing phase $\theta = \pi$ when they reach $(\theta_a(c), \eta_a(c))$.

PROPOSITION 4.1. *$\theta_a(c)$ is a monotone decreasing function of c for $c > 0$.*

Proof. We focus on the path of θ^u from θ_{rest} to $\theta_a < 0$. Recall from (13) that for each fixed $\eta < \eta_a$ we denoted the negative θ-value on the θ-nullcline by θ_-. θ_- depends on c in addition to η; we make this dependence explicit here. We now consider how far θ^u lies to the left of $\theta_-(\eta, c)$, depending on c; properly defined, a greater lag distance corresponds to a smaller (more negative) θ_a.

To do this, we use the change of variables $\theta^u = \phi + \theta_-$ for $\eta \in [0, \eta_a(c))$. By construction, since (θ^u, η^u) cannot cross θ_-, the lag $\phi < 0$ for $\eta > 0$; further, $\phi(0) = 0$ because θ^u and θ_- both tend to θ_{rest} as $\eta \to 0$. We also let $f_1(\eta, c) = -\beta - \frac{g_{syn} c}{1+c}\,\eta$. Since $\eta < \eta_a$ and $\beta \in (-1, 0)$, we have $f_1(\eta, c) \in (0, -\beta)$. Based on this notation, we note that

$$\cos(\theta_-) = \frac{1 - f_1(\eta, c)}{1 + f_1(\eta, c)} \quad \text{and} \quad \sin(\theta_-) = -\frac{2\sqrt{f_1(\eta, c)}}{1 + f_1(\eta, c)}.$$

In this new notation, (8) for θ^u becomes

$$\begin{aligned} \eta\, c \left(\frac{\partial \theta_-}{\partial \eta} + \frac{\partial \phi}{\partial \eta} \right) &= [1 - f_1(\eta, c)] + [-1 - f_1(\eta, c)] \cos(\theta_- + \phi) \\ &= [1 - f_1(\eta, c)] + [-1 - f_1(\eta, c)](\cos\theta_- \cos\phi - \sin\theta_- \sin\phi) \\ &= [1 - f_1(\eta, c)](1 - \cos\phi) - 2\sqrt{f_1(\eta, c)} \sin\phi. \end{aligned} \tag{20}$$

We can compute $\frac{\partial \theta_-}{\partial \eta}$ directly from (13):

$$\frac{\partial \theta_-}{\partial \eta} = \frac{g_{syn}\frac{c}{1+c}}{\sqrt{f_1(\eta,c)}(1+f_1(\eta,c))} \equiv -B(\eta,c). \tag{21}$$

We will follow the evolution of $\phi(\eta)$ as η increases from 0. Combining (20) and (21) yields

$$\frac{\partial \phi}{\partial \eta} = \frac{(1-f_1(\eta,c))(1-\cos\phi)}{\eta c} + \left(-\frac{2\sqrt{f_1(\eta,c)}\sin\phi}{\eta c}\right) + B(\eta,c). \tag{22}$$

Since $\phi < 0$ for $\eta > 0$ and $\phi(0) = 0$, $\partial\phi/\partial\eta$ is initially negative. Since $f_1(\eta,c) \in (0,-\beta)$ and $\phi < 0$ for $\eta > 0$, the first two terms in (22) are positive. Also, it is easy to see that they are decreasing functions of c and of η. The last term in (22) is negative, and its magnitude is an increasing function of c and of η. Consequently, $\frac{\partial\phi}{\partial\eta}$ remains negative as η increases from 0 and is a decreasing function of c. We will make use of all of these properties of the terms in (22) below.

We want to show that if $c_2 > c_1$, then for a choice of η_2, η_1 such that $\theta_-(\eta_2,c_2) = \theta_-(\eta_1,c_1)$ we have $\phi(\eta_2,c_2) < \phi(\eta_1,c_1)$, where both terms are negative by construction. This, as well as the rest of our strategy, is illustrated in Figure 12. To begin, we first integrate (22) from $\eta = 0$ to arbitrary fixed $\eta = \eta_2 < \eta_a(c_2)$. From this, we seek a preliminary upper bound for the difference $\phi(\eta_2,c_2) - \phi(\eta_2,c_1)$. To derive this bound, we can ignore the first two terms in (22), since they give positive contributions to $\partial\phi/\partial\eta$ that decrease as c increases. Thus,

$$\phi(\eta_2,c_2) - \phi(\eta_2,c_1) < \int_0^{\eta_2} B(\eta,c_2)\,d\eta - \int_0^{\eta_2} B(\eta,c_1)\,d\eta < 0. \tag{23}$$

Note from (13) that $\theta_-(\eta_2,c_2) = \theta_-(\eta_1,c_1)$ translates to

$$\frac{c_2}{1+c_2}\eta_2 = \frac{c_1}{1+c_1}\eta_1. \tag{24}$$

For fixed η_2, (24) defines η_1. Since $c_2 > c_1$, we have $\eta_1 > \eta_2$. That is, to obtain $\phi(\eta_1,c_1)$ from $\phi(\eta_2,c_2)$, we have to let $\phi(\eta,c_1)$ evolve over the extra interval $\eta_1 - \eta_2$.

By doing so, we attain a lower bound on the negative quantity $\phi(\eta_1,c_1) - \phi(\eta_2,c_1)$. Again, we ignore the positive contribution from the first two terms in (22), as they will only make $\phi(\eta_1,c_1)$ less negative. This gives us

$$\phi(\eta_1,c_1) - \phi(\eta_2,c_1) > \int_{\eta_2}^{\eta_1} B(\eta,c_1)\,d\eta. \tag{25}$$

Now we are ready to compare $\phi(\eta_2,c_2)$ and $\phi(\eta_1,c_1)$. Recall that $B = -\partial\theta_-/\partial\eta$. When we combine (23) and (25), we attain

$$\phi(\eta_2,c_2) - \phi(\eta_1,c_1) < \int_0^{\eta_2} B(\eta,c_2)\,d\eta - \int_0^{\eta_1} B(\eta,c_1)\,d\eta\ = 0, \tag{26}$$

where the difference of integrals equals 0 because $\theta_-(\eta_2,c_2) = \theta_-(\eta_1,c_1)$ by definition; see Figure 12. In particular, we can let $\eta_2 \uparrow \eta_a(c_2)$, such that $\theta_-(\eta_2,c_2) = \theta_-(\eta_1,c_1) \uparrow 0$, and then we have $\eta_1 \uparrow \eta_a(c_1)$. Then (26) gives us $\theta_a(c_2) = \phi(\eta_2,c_2) < \phi(\eta_1,c_1) =$

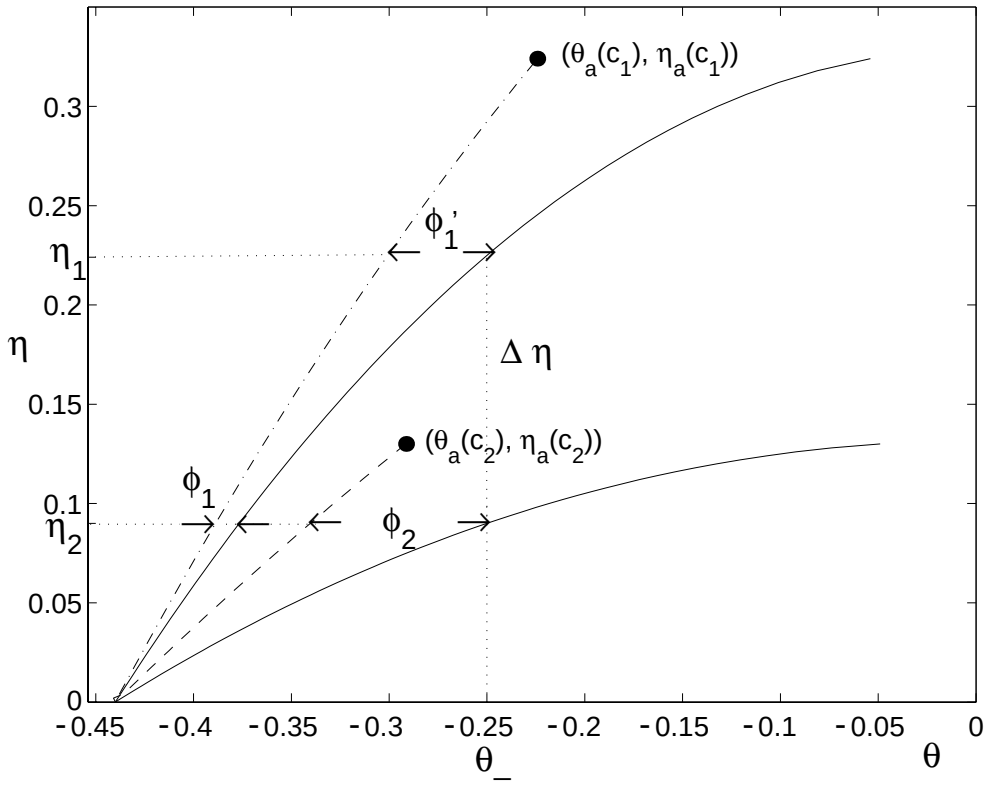

FIG. 12. *The relevant curves for the lag argument, computed numerically for* $g_{syn} = 1.9$. *The solid curves are the branches* $\theta_-(\eta, c_1)$ *and* $\theta_-(\eta, c_2)$ *of the* θ*-nullclines for* $c = c_1 = 0.08$ *and* $c = c_2 = 0.1$, *respectively; the curve for* c_1 *lies above that for* c_2. *The dashed curve represents* (θ^u, η^u) *for* $c = c_2$, *and the dash-dotted curve represents* (θ^u, η^u) *for* $c = c_1$. *The label* θ_- *on the horizontal* θ*-axis denotes* $\theta_-(\eta_2, c_2) = \theta_-(\eta_1, c_1)$. *Finally,* $\phi_1' = \phi(\eta_1, c1)$, $\phi_i = \phi(\eta_2, c_i)$ *for* $i = 1, 2$, *and* $\Delta\eta$ *denotes* $\eta_1 - \eta_2$. *The lag argument shows that* $\phi_2 < \phi_1' < \phi_1 < 0$.

$\theta_a(c_1)$ for $c_2 > c_1 > 0$, as desired. This concludes the proof of Proposition 4.1; see Figure 13 for a numerical illustration of the result.

Next, we let $\xi_{\theta_a \to \pi}(c)$ denote the time from the moment $\xi = \ln(\eta_a(c))$, when the fixed points of the θ-equation coalesce, until θ reaches the firing phase π. In other words, $\xi_{\theta_a \to \pi}$ is the time for the θ-coordinate of the unstable manifold (θ^u, η^u) to evolve from θ_a to π as (θ^u, η^u) evolves under the flow of (9).

PROPOSITION 4.2. $\xi_{\theta_a \to \pi}$ *is a monotone increasing function of* $c > 0$.

Proof. We know from Proposition 4.1 that θ_a is a monotone decreasing function of c. Renormalize time ξ for system (9) in a c-dependent way such that $\xi = 0$ when $(\theta^u(\xi; c), \eta^u(\xi; c)) = (\theta_a(c), \eta_a(c))$ for every c; these points are highlighted in Figure 12, where $c_2 > c_1$. Thus, $\theta^u(0; c)$ becomes a monotone decreasing function of c, by Proposition 4.1. Since this renormalization is simply a c-dependent translation of ξ, it does not change $d\theta/d\xi$.

Now, suppose that, for some $\bar{\xi} > 0$, it happens that $\theta^u(\bar{\xi}, c_1) = \theta^u(\bar{\xi}, c_2)$ for $c_2 > c_1 > 0$. It suffices to show that if this were to occur, then $\theta^u(\xi, c_1) > \theta^u(\xi, c_2)$ for $0 < \xi - \bar{\xi} \ll 1$. That is, to prove the proposition, it suffices to show that $\frac{\partial}{\partial c}(\frac{d\theta^u}{d\xi}) < 0$

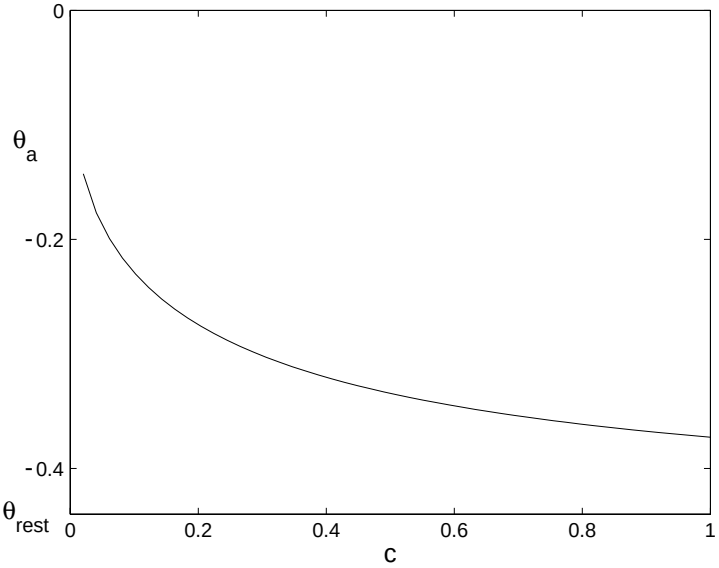

FIG. 13. *Plot of θ_a as a function of c, computed numerically with $g_{syn} = 2.0$, illustrating its monotone decreasing nature.*

at $\bar{\xi}$, with η replaced by $\eta_a(c)\eta = \eta_a(c)e^{\xi}$ to account for the dependence of initial conditions on c.

Differentiation of the θ-equation from (9) with respect to c, for fixed θ and $\eta = \eta_a(c)e^{\xi}$, yields

$$\frac{\partial}{\partial c}\left(\frac{d\theta^u}{d\xi}\right) = -\frac{f(\theta^u)}{c^2} - g(\theta^u)\left(\frac{g_{syn}\eta_a(c)}{(1+c)^2} - \frac{\beta}{(1+c)c^2}\right)e^{\xi}. \tag{27}$$

Since $d\theta/d\xi \geq 0$ at any point $(\theta, \eta_a(c))$, with equality if and only if $\theta = 0$, we know from (9) that

$$-\frac{f(\theta^u)}{c} - g(\theta^u)\frac{g_{syn}\eta_a(c)}{1+c} \leq 0 \tag{28}$$

with equality if and only if $\theta^u = 0$. The two terms on the right-hand side of (27) are obtained from the corresponding terms on the left-hand side of (28) via multiplication by different positive factors. Thus, to show that $\frac{\partial}{\partial c}(\frac{d\theta^u}{d\xi}) < 0$ at $\bar{\xi}$, it suffices to show that the factor for the second terms exceeds the factor for the first terms for $\xi = \bar{\xi}$. This yields the condition

$$\frac{1}{c} < \left(\frac{1}{1+c} - \frac{\beta}{g_{syn}c^2\eta_a(c)}\right)e^{\bar{\xi}}. \tag{29}$$

Substitution of $\eta_a(c) = -\beta(1+c)/(g_{syn}c)$ into the right-hand side of (29) reduces this inequality, after some algebra, to $1 < e^{\bar{\xi}}$, which holds since $\bar{\xi} > 0$. This concludes the proof of Proposition 4.2.

Remark 4.1. Since $\eta(0) = 1$, a traveling wave solution exists when $\xi_{\theta_a \to \pi} = \xi_{\eta_a \to 1}$, where the latter denotes the time for η^u to progress from η_a up to 1. Like θ_a, the value

η_a decreases as c increases (see (14)). Correspondingly, we can see, by integrating $d\eta/d\xi = \eta$ from $\eta = \eta_a$ up to $\eta = 1$, that

$$\xi_{\eta_a \to 1}(c) = \ln\left(\frac{g_{syn}c}{-\beta(1+c)}\right) \quad \text{with } \frac{\partial \xi_{\eta_a \to 1}(c)}{\partial c} = \frac{1}{c(1+c)} > 0.$$

That is, like $\xi_{\theta_a \to \pi}$, the time $\xi_{\eta_a \to 1}$ is a monotone increasing function of c. Thus, although it takes longer for θ to reach firing phase when c is larger, it also has a longer time available to do so before $\eta = 1$ and correspondingly $\xi = 0$. The competition of these two effects generates exactly two solutions in numerical simulations, given by two intersections of $\xi_{\theta_a \to \pi}(c)$ and $\xi_{\eta_a \to 1}(c)$, as seen in Figure 11. However, uniqueness may in theory fail through the following scenario. Suppose that, as we increase c, we go from undershoot to overshoot and back to undershoot again, obtaining two traveling wave solutions. If h subsequently experiences a sharp increase in c, then it is possible for another transition to overshoot to occur, generating additional traveling waves.

4.2. Lower bounds on the synaptic strength required for waves to exist. One of the interesting features of dynamical system (7), observed numerically, is that traveling wave solutions cannot exist if the coupling strength g_{syn} is too small. The numerical simulations shown in Figure 4 demonstrate that for a specific choice of $h(\xi, c)$ a saddle-node bifurcation occurs: two traveling wave solutions exist with different speeds for g_{syn} sufficiently large, and these coalesce into a single solution and then vanish as g_{syn} decreases. Finding the bifurcation value of g_{syn} analytically is not possible. However, here we derive an analytical lower bound for it, as a function of the parameter $\gamma := -\beta$; this also proves that traveling waves to (7) cannot exist when the coupling strength is too small.

Let θ_f denote the value of the θ-coordinate of the unstable manifold (θ^u, η^u) when $\eta^u = 1$. In theory, one would obtain a graph of the bifurcation value of g_{syn} versus γ as follows: for fixed γ, one would take the value of g_{syn} for which the maximum of θ_f over all possible wave speeds c is π. Since we cannot compute this analytically, we instead derive a lower bound on g_{syn} through the use of approximations that increase θ_f; if a value of g_{syn} is so small that the increased θ_f is less than π for all c, then the actual θ_f is less than π for this g_{syn} for all c, and no waves exist.

We split the tracking of (θ^u, η^u) into subintervals. The first interval to consider is $\eta \in [0, \eta_a]$, where η_a was defined in (14). We know that the unstable manifold is confined to the left of the θ-nullcline in (θ, η)-space. As a consequence, $\theta_a = \theta(\eta_a) < 0$. We thus make the approximation $\theta(\eta_a) = 0$, which will increase θ_f.

Starting from $\theta(\eta_a) = 0$, we next integrate (8) over $[\eta_a, \eta_T]$, defined as in subsection 3.3 such that $\theta(\eta_T) = \theta_T$, neglecting the term $f(\theta)$. Since $f(\theta) < 0$ on this interval, this gives a smaller value of η_T than would result from integrating the full equation and consequently increases θ_f, as our bounding approach allows. Neglecting $f(\theta)$ in (8) yields

$$\frac{d\theta}{d\eta} = \frac{(1+\cos(\theta))g_{syn}}{1+c}.$$

From here, by separation and integration from 0 to θ_T in θ and from η_a to η_T in η, we easily obtain

$$\eta_T = \eta_a + \frac{\sqrt{\gamma}}{g_{syn}}(1+c) = \frac{\gamma}{g_{syn}}\frac{1+c}{c} + \frac{\sqrt{\gamma}}{g_{syn}}(1+c). \tag{30}$$

Note that if $\eta_T = 1$, then $\theta_f = \theta_T < \pi$. Substitution of $\eta_T = 1$ reduces (30) to

$$-\gamma + (g_{syn} - \gamma - \sqrt{\gamma})c - \sqrt{\gamma}c^2 = 0. \tag{31}$$

We can solve for the roots of (31) to find the speeds $c_{1,2}$ at which $\eta_T = 1$ is realized. This gives

$$c_{1,2} = \frac{(g_{syn} - \gamma - \sqrt{\gamma}) \pm \sqrt{(g_{syn} - \gamma - \sqrt{\gamma})^2 - 4\gamma^{\frac{3}{2}}}}{2\sqrt{\gamma}}. \tag{32}$$

The existence of traveling waves requires $\theta_f > \theta_T$, which can only occur for $c \in (c_1, c_2)$. The two roots c_1, c_2 collide, such that the interval (c_1, c_2) ceases to exist and traveling waves cannot occur, when the term under the square root in (32) is 0. This leads to the following formula for a lower bound on the strength g_{syn} required for traveling waves to exist:

$$g_{syn} = \gamma + \sqrt{\gamma} + 2\gamma^{\frac{3}{4}}. \tag{33}$$

The discriminant is also zero when $g_{syn} = \gamma + \sqrt{\gamma} - 2\gamma^{\frac{3}{4}}$, but this is not relevant, as it gives $c_1, c_2 \leq 0$ in (32). The lower bound (33) is plotted versus γ as the dash-dotted curve in Figure 14; the numerically computed lower bound on g_{syn}, required to make $\theta_f > \theta_T$, is plotted as the dotted line for comparison.

Instead of taking $\eta_T = 1$, we can take η_T from (30) and make further approximations over the interval $[\eta_T, 1]$ that ultimately improve our lower bound on $g_{syn}(\gamma)$. However, the utility of the resulting formulas for $g_{syn}(\gamma)$ is compromised by their complexity, and they are omitted here. We obtained an additional lower bound on $g_{syn}(\gamma)$ by using (30) in numerical simulations of (9). In these simulations, for each fixed γ, solutions were followed from the initial condition (θ_T, η_T) up to $\eta = 1$, with η_T given in (30). For fixed g_{syn}, we checked whether any c values gave $\theta \geq \pi$ at $\eta = 1$. This enabled us to approximate the minimum value of g_{syn} required for any trajectories from (θ_T, η_T) to reach $(\pi, 1)$. This represents a lower bound on the g_{syn} needed for traveling waves to exist since, by construction, (θ^u, η^u) lies to the left of the trajectory through (θ_T, η_T) in the (θ, η)-plane, for all c. The resulting additional bound is plotted as a function of γ as the dashed curve in Figure 14, while the bifurcation value of $g_{syn}(\gamma)$ based entirely on numerical simulations of (9) is shown as the solid curve for comparison.

5. Discussion.

5.1. Generalizations.

The results of the previous two sections hold for general integrable J, α satisfying hypotheses (H1) and (H2). When these hold, the function $h(\xi, c)$ has the following properties:

$$\begin{cases} h(\xi, 0) = 0, & \xi < 0, \\ h(\xi, c) > 0, & c > 0,\ \xi < 0, \\ \\ h(\xi, c) \to \bar{c} \geq 0 & \text{as } c \to \infty, \\ h(\xi, c) \to 0 & \text{as } |\xi| \to \infty, \\ \\ h(\xi, c) > h(-\xi, c), & \xi > 0, \end{cases} \tag{34}$$

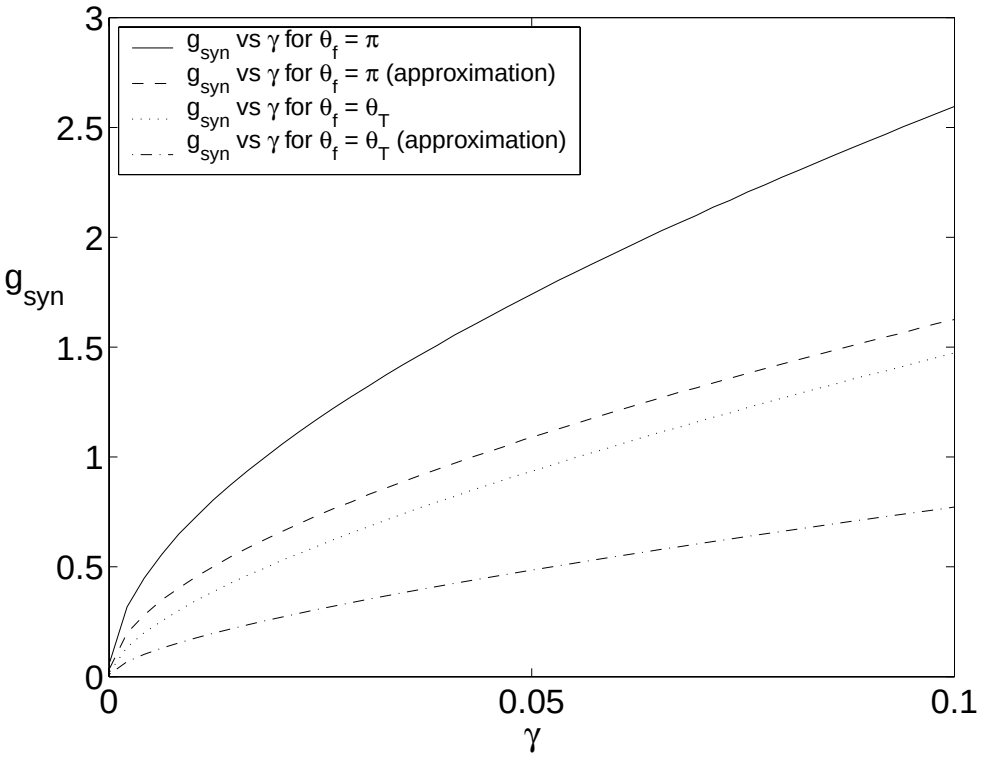

FIG. 14. *Four different estimates of the lower bound of g_{syn} needed for traveling wave solutions to* (9) *to exist. Dash-dotted curve: analytical bound from* (33). *Dotted curve: numerically computed bound on the value of g_{syn} needed for any solutions to reach θ_T before η reaches* 1. *Dashed curve: bound derived from numerical continuation of $(0, \eta_T)$ to $(\pi, 1)$, with η_T computed analytically from* (30). *Solid curve: numerically computed bound on g_{syn}.*

for a constant $\bar{c} < \infty$. In particular, the last property follows from the general expression for $h(\xi, c)$:

$$h(\xi, c) = \int_0^\infty d\xi' J(|\xi - \xi'|)\alpha(\xi'/c).$$

To see this more clearly, we use the notation:

$$\begin{cases} h^+(\xi, c) = h(\xi, c) = \int_0^\infty d\xi' J(|\xi - \xi'|)\alpha(\xi'/c), & \xi > 0, \\ h^-(\xi, c) = h(-\xi, c) = \int_0^\infty d\xi' J(|-\xi - \xi'|)\alpha(\xi'/c), & \xi > 0. \end{cases} \tag{35}$$

It can be clearly seen that $h^+(\xi, c) > h^-(\xi, c)$ for $\xi > 0$, since $|-\xi - \xi'| > |\xi - \xi'|$ and $J(\xi)$ is a decreasing function of $\xi > 0$.

With these properties, the proof of existence of traveling waves is similar to that in section 3. The asymptotic behavior of h in ξ ensures that compactification can be performed to map $(-\infty, 0]$ to $[0, 1]$. The definition of η and the term $g_{syn} A_0 \frac{c_0}{1+c_0}$ in (8) depend on the particular form of h. Nevertheless, we can still bound $\bar{\eta}(\xi_\delta)$ as in (11) by increasing g_{syn} and decreasing δ, and thus the overshoot argument holds.

Similarly, we still have the knee of the θ-nullcline at $(0, \eta_a(c))$ with $\eta_a(c) > 1$ for

c sufficiently small, since $h(\xi, 0) = 0$ for $\xi < 0$ (see (7)). Thus, we get undershoot for small velocities.

For large velocities, we can substitute any particular $h(\xi, c)$ into (16), and we get $\eta_T > 1$ for c sufficiently large since h tends to a finite asymptotic value as $c \to \infty$.

The last property in (34) ensures that, in each traveling wave solution, the system will not return to the rest state until each cell fires more than one spike.

Section 4 also carries over, but analytical formulas may become more complicated when the form of $h(\xi, c)$ necessitates the use of more complicated compactifications than $\eta = e^{\xi}$ to convert (7) to an autonomous system.

5.2. Existence of traveling waves. We have considered a model one-dimensional network of theta neurons with excitatory coupling, representing a continuum of cells that are nearby in parameter space to saddle-node bifurcations in their voltage dynamics. Using a regular, or smoothly propagating, traveling wave formulation, under the assumption that excited cells fire only single spikes and then return to rest, we have derived a differential equation for traveling wave solutions. The single spike assumption affects the form of coupling function $h(\xi, c)$ in the equation. We have employed a shooting argument to prove the existence of two traveling wave solutions to this equation, a fast wave and a slow wave, when the synaptic coupling conductance g_{syn} is sufficiently large; note that g_{syn} is a parameter that can be varied independently of h. Since coupling is excitatory, additional spikes would lead to a more positive form of h; hence, these results also imply the existence of two traveling waves (with different speeds from the originals) without the single-spike assumption; see Remark 3.1. These results are consistent with the findings of Golomb and Ermentrout [10] for a one-dimensional network of integrate-and-fire neurons with excitatory coupling.

We also have proved that when a cell at the leading edge of an existing wave receives the form of coupling corresponding to the single-spike assumption, this coupling will be sufficient to force the cell to fire more than one spike before returning to rest. This shows that the network model considered here does not support traveling waves in which each cell in the continuum fires only a single spike. Moreover, it agrees with numerical simulations (e.g., Figure 3(a)), in which multiple spikes are always observed in this model. Analysis of how many additional spikes each cell fires is beyond the scope of this work, as it requires removal of the single-spike assumption, which leads to more complicated traveling wave equations. A form of synaptic depression could be implemented that affects only the form of the synaptic coupling $s(x, t)$, and thus $h(\xi, c)$, to achieve single spiking (e.g., Figure 3(b)). For example, if this adaptation left h unchanged from the form considered here for negative ξ but made h weaker for positive ξ (or even in ξ), then our shooting arguments would still hold, but single spiking would result (see Figure 10). Alternatively, inclusion of an afterhyperpolarization in the intrinsic theta neuron dynamics would make cells more refractory [4]. Sufficiently strong afterhyperpolarization would prevent each cell from firing more than one spike.

In summary, our results rigorously establish that at least two regular traveling wave solutions exist for a one-dimensional network of theta neurons. In these solutions, cells fire more than one spike before returning to rest.

5.3. Further results. Our analysis shows that solutions are created by a balance of two competing effects as the wave speed c varies. One effect is that the knee of the θ-nullcline, (θ_a, η_a), for system (9) drops towards $\eta = 0$ as c increases, and thus cells can get beyond threshold faster. The other effect is that θ increases more slowly,

relative to η, as c increases, and thus it takes longer for cells to spike. In the notation of section 4, the two times $\xi_{\theta_a \to \pi}$ and $\xi_{\eta_a \to 1}$ both increase with c.

When c is sufficiently small, $\xi_{\eta_a \to 1} = 0 < \xi_{\theta_a \to \pi}$. The existence of two traveling waves implies that $\xi_{\eta_a \to 1}$ intersects $\xi_{\theta_a \to \pi}$ at least twice as c increases. We do not have a uniqueness theorem because we have not ruled out additional intersections, although we have not observed these numerically, at least for the form of α-function that we have considered.

The traveling waves exist for g_{syn} sufficiently large. We give an analytical lower bound for the minimum value of g_{syn} for which traveling waves exist. Sharper analytical estimates can be derived, but the complexity of the resulting expressions compromises their utility. Derivation of a useful analytical upper bound on this minimum g_{syn} also remains open, as does analytical computation of the speeds at which waves exist. Note that wave speed depends on the form of $J(x), \alpha(t)$ used to couple the neurons in the network. For exponentially decaying J and α, faster decay rates correspond to weaker coupling, which would be expected to slow down the fast wave; this is borne out numerically (Figure 6).

Our results generalize to a wide class of coupling functions J and α. These include the most common biologically motivated forms of J, namely a Gaussian, exponential, or step function, and of α, namely an exponentially decaying function or a difference of two exponentials. Consideration of traveling waves in a model one-dimensional network of conductance-based Type I neurons, governed by Morris–Lecar or similar equations, should follow analogously.

Finally, we do not analyze stability of the traveling wave solutions for this system. Recent work has begun to consider linearized stability of traveling waves in conductance-based networks with continuous coupling [20]. However, results are limited to cases in which eigenvalue problems take the form of nonautonomous ordinary differential equations with limited nonlocal terms. Here, the stability problem derived from linearization of (6) about a traveling wave solution is a fully nonlocal integro-differential equation.

Acknowledgments. Remus Osan thanks Tanase Costin for helpful discussions and suggestions. All three authors also thank the referees for useful comments that improved the presentation of this work.

REFERENCES

[1] P. C. Bressloff, *Synaptically generated wave propagation in excitable neural media*, Phys. Rev. Lett., 82 (1999), pp. 2979–2982.

[2] B. W. Connors and Y. Amitai, *Generation of eliptiform discharge by local circuits of neocortex*, in Epilepsy: Models, Mechanisms and Concepts, P. A. Schwartkroiun, ed., Cambridge University Press, Cambridge, UK, 1993, pp. 388–423.

[3] A. Destexhe, T. Bal, D. A. McCormick, and T. Sejnowski, *Ionic mechanisms underlying synchronized oscillations and propagating waves in a model of ferret thalamic slices*, J. Neurophysiol., 76 (1996), pp. 2049–2070.

[4] B. Ermentrout, M. Pascal, and B. Gutkin, *The effects of spike frequency adaptation and negative feedback on the synchronization of neural oscillators*, Neural Comput., 13 (2001), pp. 1285–1310.

[5] G. B. Ermentrout, *Type I membranes, phase resetting curves, and synchrony*, Neural Comput., 8 (1996), pp. 979–1001.

[6] G. B. Ermentrout, *The analysis of synaptically generated traveling waves*, J. Comp. Neurosci., 5 (1998), pp. 191–208.

[7] G. B. Ermentrout and N. Kopell, *Parabolic bursting in an excitable system coupled with a slow oscillation*, SIAM J. Appl. Math., 46 (1986), pp. 233–253.

[8] D. Golomb, X.-J. Wang, and J. Rinzel, *Propagation of spindle waves in a thalamic slice model*, J. Neurophysiol., 75 (1996), pp. 750–769.
[9] D. Golomb and Y. Amitai, *Propagating neuronal discharges in neocortical slices: Computational and experimental study*, J. Neurophysiol., 78 (1997), pp. 1199–1211.
[10] D. Golomb and G. B. Ermentrout, *Continuous and lurching traveling pulses in neuronal networks with delay and spatially decaying connectivity*, Proc. Natl. Acad. Sci. USA, 96 (1999), pp. 13480–13485.
[11] F. C. Hoppensteadt and E. Izhikevich, *Weakly Connected Neural Networks*, Springer-Verlag, New York, 1997.
[12] U. Kim, T. Bal, and D. A. McCormick, *Spindle waves are propagating synchronized oscillations in the ferret LGNd in vitro*, J. Neurophysiol., 74 (1995), pp. 1301–1323.
[13] R. Metherate and S. J. Cruikshank, *Thalamocortical inputs trigger a propagating envelope of gamma-band activity in auditory cortex in vitro*, Exp. Brain Res., 126 (1999), pp. 160–174.
[14] R. Osan and G. B. Ermentrout, *Two dimensional synaptically generated traveling waves in a theta-neuron neural network*, Neurocomputing, 38–40 (2001), pp. 789–795.
[15] R. Miles, R. D. Traub, and R. K. S. Wong, *Spread of synchronous firing in longitudinal slices from the CA3 region of the hippocampus*, J. Neurophysiol., 60 (1995), pp. 1481–1496.
[16] J. C. Prechtl, L. B. Cohen., P. P. Mitra, and D. Kleinfeld, *Visual stimuli induce waves of electrical activity in turtle cortex*, Proc. Natl. Acad. Sci. USA, 94 (1997), pp. 7621–7626.
[17] J. Rinzel and J. B. Keller, *Traveling wave solutions of a nerve conduction equation*, Biophys. J., 13 (1973), pp. 1313–1337.
[18] J. Rinzel, D. Terman, X.-J. Wang, and B. Ermentrout, *Propagating activity patterns in large-scale inhibitory neuronal networks*, Science, 279 (1998), pp. 1351–1355.
[19] D. H. Terman, G.B. Ermentrout, and A. C. Yew, *Propagating activity patterns in thalamic neuronal networks*, SIAM J. Appl. Math., 61 (2001), pp. 1578–1604.
[20] D. Terman and L. Zhang, *Asymptotic Stability of Traveling Wave Solutions of a Singularly Perturbed System of Integral Differential Equations from Neuronal Networks*, preprint.
[21] R. D. Traub, J. G. Jefferys, and R. Miles, *Analysis of the propagation of disinhibition-induced after-discharges along the guinea-pig hippocampal slice in vitro*, J. Physiol., 472 (1993), pp. 267–287.
[22] R. D. Traub and R. Miles, *Neuronal Networks of the Hippocampus*, Cambridge University Press, Cambridge, UK, 1991.
[23] J.-Y. Wu, Y. Tsau, and L. Guan, *Propagating activation during oscillations and evoked response in neocortical slices*, J. Neurosci., 19 (1999), pp. 5005–5015.